

Balance of Calcineurin A α and CDK5 Activities Sets Release Probability at Nerve Terminals

Sung Hyun Kim^{1,2} and Timothy A. Ryan¹

¹Department of Biochemistry, Weill Cornell Medical College, New York, New York 10065 and ²Neurodegeneration Control Research Center, Age-related and Brain Disease Research Center, Department of Neuroscience, School of Medicine, Kyung Hee University, Seoul, South Korea

The control of neurotransmitter release at nerve terminals is of profound importance for neurological function and provides a powerful control system in neural networks. We show that the balance of enzymatic activities of the α isoform of the phosphatase calcineurin (CNA α) and the kinase cyclin-dependent kinase 5 (CDK5) has a dramatic influence over single action potential (AP)-driven exocytosis at nerve terminals. Acute or chronic loss of these enzymatic activities results in a sevenfold impact on single AP-driven exocytosis. We demonstrate that this control is mediated almost entirely through Cav2.2 (N-type) voltage-gated calcium channels as blocking these channels with a peptide toxin eliminates modulation by these enzymes. We found that a fraction of nerve terminals are kept in a presynaptically silent state with no measurable Ca²⁺ influx driven by single AP stimuli attributable to the balance of CNA α and CDK5 activities because blockade of either CNA α or CDK5 activity changes the proportion of presynaptically silent nerve terminals. Thus, CNA α and CDK5 enzymatic activities are key determinants of release probability.

Introduction

In the last decade cyclin-dependent kinase 5 (CDK5) has been shown to play important roles in brain function (Dhavan and Tsai, 2001), including development (Kwon and Tsai, 2000; Gupta and Tsai, 2003), signaling (Bibb et al., 1999), plasticity (Odajima et al., 2011), and neuropathology (Cruz and Tsai, 2004), whereas calcineurin (CN) (Sun et al., 2010) is important for learning and memory and signaling (Malleret et al., 2001; Zeng et al., 2001) and it also controls the phosphorylation state of a number of endocytic proteins (Cousin and Robinson, 2001). Recently, we showed that the proline-directed serine–threonine kinase CDK5 and the Ca²⁺-dependent phosphatase CN potently regulate the size of the synaptic vesicle pool that participates in neurotransmission (Kim and Ryan, 2010). Such modulation is thought to be important for bouts of sustained activity in which vesicle availability might be limiting. Responses to single action potentials (APs), i.e., release probability, is controlled by a combination of the number of release-ready vesicles and the amount and proximity of calcium influx near release sites. Recently, it was demonstrated that Cav2.2 (N-type) voltage-gated calcium channels

(VGCCs) can be phosphorylated *in vitro* by CDK5, and expression of Cav2.2 in which these phosphorylation sites are mutated to alanine diminishes synaptic performance compared with wild-type (WT) Cav2.2 when expressed in hippocampal neurons (Su et al., 2012). Therefore, we wondered whether or not the release probability at nerve terminals might be set by the integration of competing kinase and phosphatase activities on VGCCs. We investigated the potential role of these enzymes in single AP (1AP)-triggered exocytosis, taking advantage of recent improvements in optical methods to probe synapse function and synaptic calcium influx in this stimulus regimen (Ariel and Ryan, 2010; Ariel et al., 2012; Hoppa et al., 2012). To examine possible contributions of these enzymes in controlling release probability, we made use of a combination of pharmacological and/or shRNA-mediated ablation of catalytic subunits of CN and CDK5 gene expression. We show here that the α isoform of calcineurin A (CNA α) and CDK5 profoundly influence exocytosis and calcium influx even for 1AP stimuli. However, our results are in direct contradiction to what would be predicted from the *in vitro* phosphorylation results, in which loss of kinase activity would be predicted to increase synaptic calcium channel function and loss of CN activity would be predicted to enhance synaptic calcium channel function (Su et al., 2012). In contrast, we found that removal of CN activity dramatically reduces AP-driven calcium influx and exocytosis, whereas suppression of CDK5 activity leads to a large potentiation of calcium influx and exocytosis. Both of these forms of regulation are mediated almost entirely through Cav2.2 VGCCs, because simultaneous blockade of Cav2.2 with a peptide toxin ablates control by either enzyme. Furthermore, we show that the balance of these activities likely varies across synapses, because a portion of nerve terminals are kept in a completely silent state by CDK5-mediated inhibition of Ca²⁺ influx. Our results stand in contrast to the recent claim that phosphorylation of Cav2.2 en-

Received Sept. 7, 2012; revised March 13, 2013; accepted April 3, 2013.

Author contributions: S.H.K. and T.A.R. designed research; S.H.K. performed research; S.H.K. analyzed data; S.H.K. and T.A.R. wrote the paper.

This work was supported in part by National Institutes of Health Grants NS036942 and MH085783 (T.A.R.) and a sponsored research agreement with Galenea Corp. (Cambridge, MA). T.A.R. is a consultant with Galenea Corp., which provided some financial support for the work reported here. We thank Jeremy Dittman and members of the Ryan laboratory for valuable discussions. We thank Ricky Kwan, Yogesh Gerra, and Julia Marrs for excellent technical assistance. vG-pH was a gift from Rob Edwards and Susan Voglmaier (University of California, San Francisco, San Francisco, CA), and phycin-GCaMP3 was a gift from Loren Looger (Howard Hughes Medical Institute, Janelia Farms, Ashburn, VA).

Correspondence should be addressed to Timothy A. Ryan, Department of Biochemistry, Weill Cornell Medical College, Room E-107, 1300 York Avenue, New York, NY 10065. E-mail: taryan@med.cornell.edu.

DOI:10.1523/JNEUROSCI.4288-12.2013

Copyright © 2013 the authors 0270-6474/13/338937-14\$15.00/0

hances synaptic function (Su et al., 2012) and suggest that alternate CDK5 phosphorylation sites of either Cav2.2 or another protein that controls Cav2.2 is critical in determining synaptic performance.

Materials and Methods

Cell culture and optical setup. Hippocampal CA3–CA1 regions were dissected from 1- to 2-d-old Sprague Dawley rats, dissociated, and plated onto poly-ornithine-coated glass for 14–21 d as described previously (Ryan, 1999). All constructs were transfected 7–8 d after plating. Experiments were performed 14–21 d after plating (6–13 d after transfection), and the coverslips were mounted in a rapid-switching, laminar-flow perfusion and stimulation chamber (volume, $\sim 75 \mu\text{l}$) on the stage of a custom-built laser illuminated epifluorescence microscope. Live-cell images were acquired with an Andor iXon+ (model DU-897E-BV) back-illuminated EM CCD camera. A solid-state diode pumped 488 or 561 nm lasers [for mCherry (mCh) excitation] that were shuttered using acousto-optic tunable filters. Fluorescence excitation and collection was done through a 40 \times , 1.3 numerical aperture Fluor Carl Zeiss objective and a 1.6 \times Optivar using 515–560 nm emission and 510 nm dichroic filters (for pHluorin, Fluo5F, or GCaMP3) and a 572–647 nm emission filter (for mCh). APs were evoked by passing 1 ms current pulses, yielding fields of $\sim 10 \text{ V/cm}$ via platinum–iridium electrodes. Cells were continuously perfused (0.2 ml/min) in a saline solution containing 119 mM NaCl, 2.5 mM KCl, 2 mM CaCl $_2$, 2 mM MgCl $_2$, 25 mM HEPES, buffered to pH 7.4, 30 mM glucose, 10 μM 6-cyano-7-nitroquinoxaline-2,3-dione, and 50 μM D,L-2-amino-5-phosphonovaleric acid. For buffer containing 4 or 1.2 mM Ca $^{2+}$ concentration for measuring one AP (1AP), Mg $^{2+}$ was substituted for a constant divalent concentration. Temperature was clamped at 30°C to decrease effects arising from temperature fluctuations. Unless otherwise noted, all chemicals were obtained from Sigma except for Ca $^{2+}$ channel toxins, ω -agatoxin IVA, ω -conotoxin GVIA (Alomone Labs), ionomycin (Alomone Labs), Ca $^{2+}$ dyes, Fluo5F-AM, magnesium green-AM (MgGreen-AM) (Invitrogen), and EGTA-AM (Invitrogen). NH $_4$ Cl applications were done with 50 mM NH $_4$ Cl in substitution of 50 mM NaCl, buffered to pH 7.4. Roscovitine (Calbiochem) was used at 50 μM , and cyclosporin A (CSA) was used at 30 μM for 30 min when indicated. Anti-synapsin antibodies were obtained from Synaptic Systems, and anti-CNA α and anti-CNA β antibodies were a gift from Galenea Corp.

Imaging and analysis of 1AP-driven Ca $^{2+}$ influx. Measurements of 1AP Ca $^{2+}$ influx at nerve terminals were performed using three different Ca $^{2+}$ indicators: Fluo5F-AM, MgGreen-AM, and GCaMP3 (Tian et al., 2009) fused to synaptophysin. For high-speed (1000 or 1 kHz) imaging with Fluo5F, vesicle-associated membrane protein 2 (VAMP2)–mCh-transfected neurons were loaded with Fluo5F-AM (5 μM) for 10 min and flowed by a 20 min wash period (Hoppa et al., 2012). For imaging of 1AP Ca $^{2+}$ influx at soma, cytosolic mKate2 (red fluorescence)-transfected neurons were loaded with Fluo5F-AM. mKate2-positive whole soma areas were selected as a region of interest for analysis. Imaging of Ca $^{2+}$ influx stimulated by 1APs was acquired at 1 kHz by integrating for 975 μs over a reduced region of the EM CCD chip (crop mode) that had been defined using a physical mask in an intermediate image plane in the collection path. EGTA-AM was applied for 120 s, and CSA or roscovitine was applied for 30 min, although the impact of roscovitine was usually noticed within the first few minutes of application. 1AP responses were obtained by averaging 10 trials (spaced 30 s apart) over 5–10 boutons from a single cell in 4 or 1.2 mM external Ca $^{2+}$. For MgGreen, VAMP2–mCh-transfected cells were loaded with 20 μM MgGreen-AM for 10 min and flowed by a 20 min wash period as described previously (Ariel and Ryan, 2010). Imaging of Ca $^{2+}$ influx by 1 AP was acquired at 100 Hz by integrating for 9.74 ms in frame transfer mode. For GCaMP3, at the end of each experiment, ionomycin (200 μM) was applied to measure maximum fluorescence of Physin–GCaMP3. 1AP responses were obtained by averaging 10–15 trials (spaced 30 s apart) over 20–30 boutons from a single cell in 4 mM external Ca $^{2+}$. The P/Q-type VGCC blocker (ω -agatoxin IVA, 400 nM) and N-type VGCC blocker (ω -conotoxin GVIA, 1 μM) were applied for 2 min and washed out before AP stimulation.

Images were analyzed in NIH ImageJ using a custom-written plugin. Fluorescence time course traces were analyzed using Origin Pro (version 7.5 or 8.0). For analysis of Ca $^{2+}$ dye, Fluo5F, or MgGreen, only VAMP2–mCh-positive areas (boutons) are selected as a region of interest. ΔF values of each 1AP trial were subtracted with local background and were averaged. The peak amplitude was taken and normalized by F_0 . For analysis of genetic Ca $^{2+}$ indicator, 1AP response amplitudes were obtained by averaging 10–15 trials. The peak was averaged for frames 2–7 after the stimulus. This value was normalized by peak of ionomycin fluorescence and subjected to an equation for converting to linearized value of GCaMP3, because GCaMP3 signals are known to be nonlinear (Tian et al., 2009). We corrected for this through a linearization process described below.

Imaging and analysis of 1AP-driven vesicle release with vesicular glutamate transporter–pHluorin. To measure vesicle release, neurons were transfected with vesicular glutamate transporter–pHluorin (vG–pH) with/without shRNA–CDK5 or shRNA–CNA α . 1AP responses were obtained by averaging 10 trials (spaced 30 s apart) over 20–30 boutons from a single cell in 4 or 1.2 mM external Ca $^{2+}$ in the absence or presence of roscovitine or CSA. Images were acquired at 20 or 100 Hz by integrating for 20 or 9.74 ms in frame transfer mode. Images were analyzed using NIH ImageJ and Origin Pro. All visible varicosities were selected for analysis by testing their responsiveness to test application of NH $_4$ Cl. To estimate 1AP-driven responses of vG–pH, the peak regions of 1AP are taken and normalized to the maximum fluorescence obtained during an NH $_4$ Cl application. NH $_4$ Cl were analyzed by mean value of plateau regions. Finally, these peak values of 1AP in various conditions are normalized to the 1AP peak value of WT. In the case of CSA application, we found that, in $\sim 50\%$ of cells, application of CSA led to a spontaneous increase in vG–pH fluorescence, making additional experiments impossible. These were excluded from additional experimental analysis.

Comparison of changes in exocytosis and calcium influx with previously determined cooperativity curve. We previously determined 1AP-driven exocytosis measured with vG–pH as a function of the relative calcium entry measured in separate experiments for conditions in which calcium entry was varying (Ariel and Ryan, 2010). The normalized solid curve shown in Figure 4 is described by $y = x^{3.4}/(1.9 + x^{3.4})$, where y is the normalized value of exocytosis and x is the calcium entry relative to that obtained at 2 mM external calcium. We previously determined the value of exocytosis and calcium influx for 4 mM external calcium on this curve and then use this as a reference point for plot the impact of CDK5 or CN blockade. For data at 1.2 mM calcium, we compared the exocytosis and calcium influx values with that obtained at 4 mM external calcium.

Other images and data analyses. Silent boutons were defined as those in which the response of 1AP was smaller than the 1 SD of the baseline before stimulation. To quantify the efficiency of knockdown (KD) of CNA α and CNA β , neurons cotransfected with shRNA–CNA α or shRNA–CNA β and GFP or vG–pH were fixed with 4% paraformaldehyde and incubated with anti-CNA α or CNA β antibodies, and subsequently Alexa Fluor-546-conjugated secondary antibodies were incubated as described previously (Kim and Ryan, 2009). Quantification of shRNA-mediated KD of CNA α and CNA β were measured by comparing the fluorescence intensity of immunostained cell bodies corrected for background in surrounding area with respect to that obtained in nontransfected neighboring neurons. The normalized intensities in KD neurons measured in this way were $[\text{CNA}\alpha]_{\text{CNA}\alpha\text{KD}} = 0.22 \pm 0.03$ ($n = 9$) and $[\text{CNA}\beta]_{\text{CNA}\beta\text{KD}} = 0.20 \pm 0.03$ ($n = 12$).

All data are presented as mean \pm SEM. Student's t test between two groups was used for statistical tests.

Conversion of GCaMP3 to linearized value. *In vitro* measurements of GCaMP3 Ca $^{2+}$ binding showed that the relationship between fluorescence and Ca $^{2+}$ concentration is nonlinear with a Hill coefficient of 2.5 (Tian et al., 2009). *In situ* calibrations obtained by comparing MgGreen signals with GCaMP3 signals showed a very similar relationship (Hoppa et al., 2012). Our *in situ* calibration allowed us to linearize the GCaMP3 signals and express them relative to the signal obtained by a 1AP using MgGreen. The expression level of GCaMP3 was normalized by comparing all responses to a saturating signal obtained by applying ionomycin (F_{MAX}) at the end of experiments. Peak fluorescence (ΔF) for each stim-

ulation was found by averaging the five highest points after stimulation and subtracting the average of 10 points before stimulation. Linearized GCaMP3 was obtained from the following equation: Linearized GCaMP3 = $\frac{((\Delta F/F)/F_{MAX}) \times k^n}{(1 - ((\Delta F/F)/F_{MAX}))^{(1/n)}}$, where $k = 9.077$ and $n = 2.46$. These latter parameters were obtained from our *in situ* Hill fit comparing MgGreen and GCaMP3 and are in excellent agreement with the *in vitro* estimate (Tian et al., 2009).

Plasmids. Physin–GCaMP3 was kindly provided by Loren Looger (Janelia Farm Research Campus, Howard Hughes Medical Institute, VA) (Tian et al., 2009). Synthetic oligonucleotides containing cDNA target sequences of rat *cna α* (GGATTCTCACCACAACAT), *cna β* (GAGTGTGTCTTGTATTAT), and rat *cdk5* (CCTCCGGGAGATCTGTCTACTCAAA) (Kim and Ryan, 2010) were cloned, annealed, and ligated into pSUPER (Invitrogen) with BglII and HindIII enzyme sites according to the instructions of the manufacturer.

Results

Loss of CNA α suppresses exocytosis at nerve terminals

Previously, we showed that CN was a potent regulator of presynaptic function, including AP-triggered exocytosis, making use of shRNA targeting the obligate regulatory subunit [calcineurin B (CNB)]. To investigate the mechanism of CN action in detail, we sought to determine which catalytic isoform of CN might be responsible for controlling AP-triggered exocytosis efficiency. In mammals, CN is composed of a regulatory subunit, CNB, encoded by a single gene and one of three isoforms of a catalytic subunit, CNA, encoded by different genes (α , β , and γ) (Klee et al., 1998). CNA α and CNA β represent the most abundant of the three catalytic subunits in brain, and both are present at nerve terminals (Fig. 1A,B). Transfection with shRNAs specifically targeting these subunits resulted in $\sim 80\%$ suppression of expression in individual primary hippocampal neurons (see Materials and Methods). To examine exocytosis, we coexpressed individual shRNAs with vG–pH. This latter reporter construct provides high-fidelity measurements of exocytosis at nerve terminals, making use of the all-or-none quenching of pHluorin by protons with a pKa of ~ 7.1 . When targeted to nerve terminals by fusion into an intraluminal loop of vG, pHluorin is mostly quenched in the resting acidic state of the synaptic vesicle but the quenching is relieved during exocytosis and equilibration of vesicle pH with the more alkaline extracellular environment. In control neurons transfected with vG–pH alone a burst of 100 APs at 10 Hz leads to a rapid rise in vG–pH fluorescence (Fig. 1C), corresponding to $\sim 15\%$ of the maximal possible value as assessed with brief NH $_4$ Cl application. In contrast, neurons coexpressing shRNA targeting CNA α and vG–pH showed much smaller responses with approximately fivefold lower exocytosis signal, corresponding to only $\sim 2.5\%$ of the NH $_4$ Cl-driven maximal fluorescence (Fig. 1C–E). In contrast, neurons coexpressing shRNA targeting CNA β were indistinguishable from controls (Fig. 1C–E). Thus, despite the presence of both CNA α and CNA β at nerve terminals, only CNA α appears critical for robust AP-triggered exocytosis. Single bouton analysis showed that the suppression in exocytosis was a general trend across the entire population of nerve terminals (Fig. 1F).

Potent control of 1AP exocytosis by CDK5 and CNA α

During repetitive AP firing, the total amount of exocytosis can in principle be regulated at several different steps, including release probability and readily-releasable pool refilling. We therefore examined exocytosis in response to 1AP stimulation to narrow down possible targets of CN function. vG–pH measurements of 1AP-driven exocytosis showed that loss of CNA α led to 1AP responses that were only $\sim 25\%$ compared with controls (Fig.

2A,B). Because our previous studies on CN regulation of presynaptic function also showed that CDK5 served to counteract CN function, we examined 1AP exocytic responses when CDK5 expression was ablated by shRNA targeting. These experiments revealed that suppression of CDK5 leads to a potent 60% potentiation of exocytosis for 1AP stimuli (Fig. 2A,B). Similar results were obtained after acute application of the small-molecule CDK5 inhibitor roscovitine (Meijer et al., 1997) (Fig. 2B). Furthermore, the ability of roscovitine to potentiate exocytosis was eliminated in neurons in which CN function was also eliminated via shRNA-mediated ablation of CNA α (Fig. 2C,D) or pharmacological block of CN using CSA (Fig. 2E,F). These data all support the idea that CDK5-mediated phosphorylation of a presynaptic substrate suppresses release probability, whereas CNA α -mediated dephosphorylation of a presynaptic substrate enhances release probability.

CNA α and CDK5 control of release probability is mediated through Cav2.2 VGCCs

Neurotransmitter release at hippocampal nerve terminals is driven by a combination of Cav2.2 (N-type) and Cav2.1 (P/Q-type) VGCCs (Takahashi and Momiyama, 1993). Application of the specific Cav2.1 blocker ω -agatoxin IVA led to an $\sim 50\%$ inhibition of 1AP-driven exocytosis, whereas application of the Cav2.2 blocker ω -conotoxin GVIA suppressed $\sim 70\%$ of exocytosis (Fig. 2G), in agreement with previous results obtained in this system (Ariel et al., 2012). In neurons in which CNA α expression has been suppressed, only agatoxin, but not conotoxin, could further reduce exocytosis (Fig. 2H). Similarly, acute application of roscovitine to block CDK5 activity showed full potentiation of exocytosis in the presence of agatoxin (Fig. 2I) but showed no effect when Cav2.2 channels were blocked (Fig. 2J). We conclude that the control of AP-triggered exocytosis by CNA α and CDK5 requires Cav2.2 calcium channel function.

CNA α and CDK5 control AP-triggered Ca $^{2+}$ influx at nerve terminals

Exocytosis at nerve terminal is tightly controlled by Ca $^{2+}$ influx via VGCCs, and the elimination of CDK5 and CNA α modulation of exocytosis by selective blockade of Cav2.2 strongly suggests that the profound modulation of exocytosis we observed occurs through modulation of calcium influx at nerve terminals. To test this hypothesis, we measured intracellular calcium ([Ca $^{2+}$]) at synaptic boutons in response to 1APs using a recently developed approach (Hoppa et al., 2012) with the fast fluorescent indicator of Ca $^{2+}$, Fluo5F-AM, sampled at 1 kHz and visualized by expression of VAMP–mCh (Fig. 3A, left). This approach led to very robust 1AP signals (Fig. 3B, black traces). However, even at millisecond time resolution, the peak signal can potentially reflect both the influx of Ca $^{2+}$ and dissipative mechanisms, such as extrusion and diffusion. To minimize the contributions of the latter, we artificially accelerated the decay time of the Ca $^{2+}$ signal ~ 10 -fold by addition of a high concentration of the mobile Ca $^{2+}$ buffer EGTA-AM. For all conditions used, this led to a suppression of the pre-EGTA peak signal by $\sim 50\%$ and a fluorescence decay time ~ 8 ms (Fig. 3B). Because the decay time of the Ca $^{2+}$ signal is now under extrinsic control, the peak signals can more safely be interpreted as a much purer reflection of calcium influx. To determine how either CN or CDK5 might influence Ca $^{2+}$ influx, we made use of acute pharmacological inhibitors as well as shRNA-mediated genetic ablation of these enzymatic activities using the above measurement strategy. These experiments showed that acute suppression of CN by addition of the CN in-

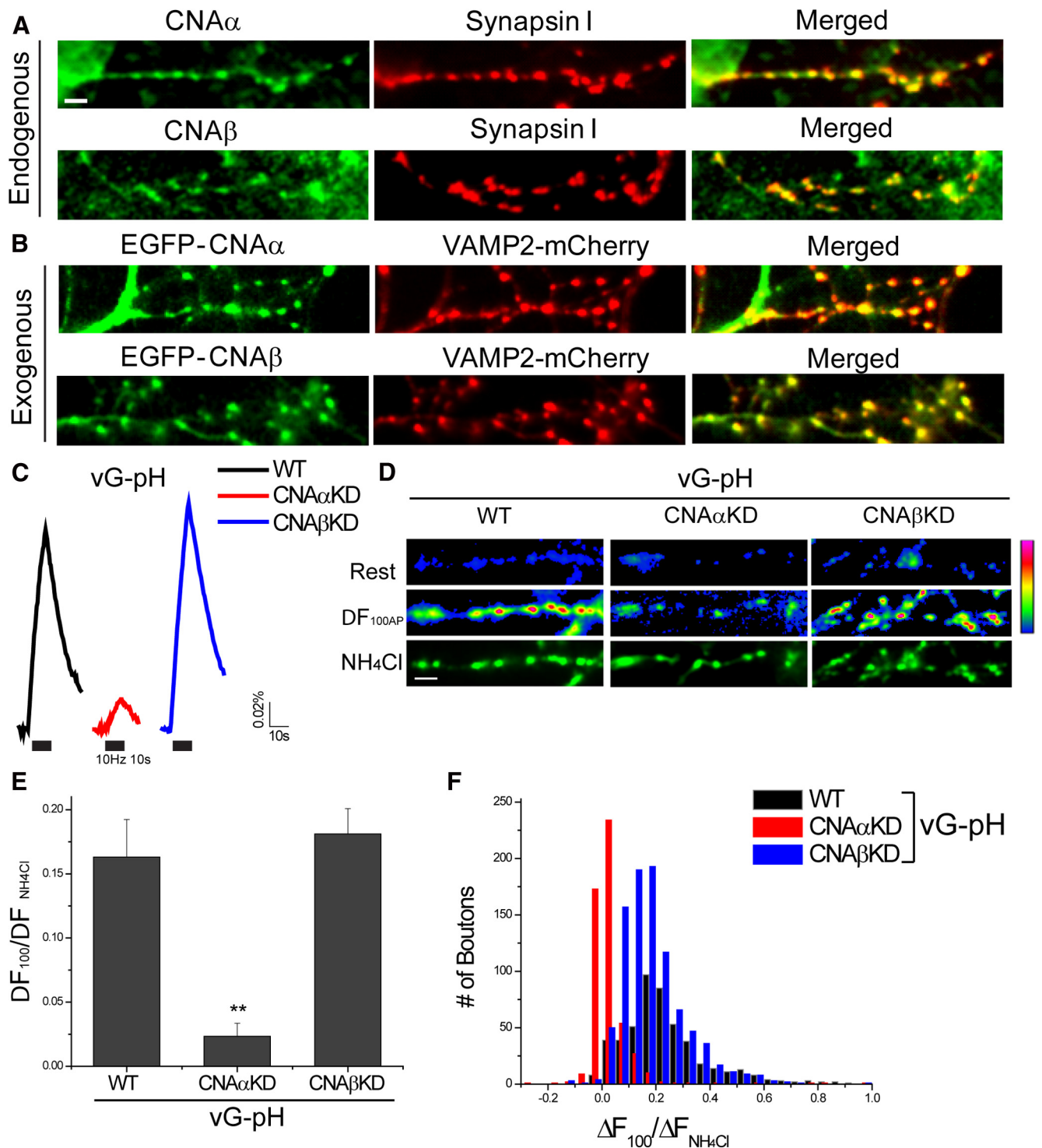


Figure 1. Ablation of CNA α not CNA β in hippocampal synapses impairs synaptic AP stimulate exocytosis. **A**, Representative images of CNA α , CNA β , and synapsin I immunostaining. Mature (14–18 d *in vitro*) neurons were fixed and costained with anti-CNA α antibody (green) and anti-synapsin I (red) (top) or anti-CNA β antibody (green) and anti-synapsin I (red) (bottom) and subsequently applied by appropriate secondary antibodies. Scale bar, 5 μ m. **B**, EGFP-CNA α (top) or EGFP-CNA β (bottom) with the presynaptic terminal marker (VAMP2-mCh) transfected into neurons. **C**, Ensemble average traces of vG-pH responses to 100 AP stimulation at 10 Hz from WT (black), CNA α (red), and CNA β (blue) depleted neurons. Intensities of vG-pH were normalized to the peak of a subsequent NH₄Cl response (total vesicle pool). **D**, Representative field of vG-pH fluorescence images at rest, the difference image for 100 AP stimulation (ΔF_{100AP}), and during NH₄Cl application in WT, CNA α KD, or CNA β KD neurons. Scale bar, 5 μ m. Average 100 AP (ΔF_{100AP}) response is significantly lower in CNA α KD but is unchanged in CNA β KD neurons. **E**, Mean values of 100 AP vG-pH response amplitudes in WT, CNA α KD, or CNA β KD neurons. WT_{100AP} = 0.163 ± 0.029 ($n = 7$), CNA α KD_{100AP} = 0.023 ± 0.010 ($n = 9$), and CNA β KD_{100AP} = 0.181 ± 0.060 ($n = 10$). ** $p < 0.01$. **F**, The 100 AP vG-pH response amplitude distribution from single boutons from WT (black), CNA α KD (red), and CNA β KD (blue) neurons.

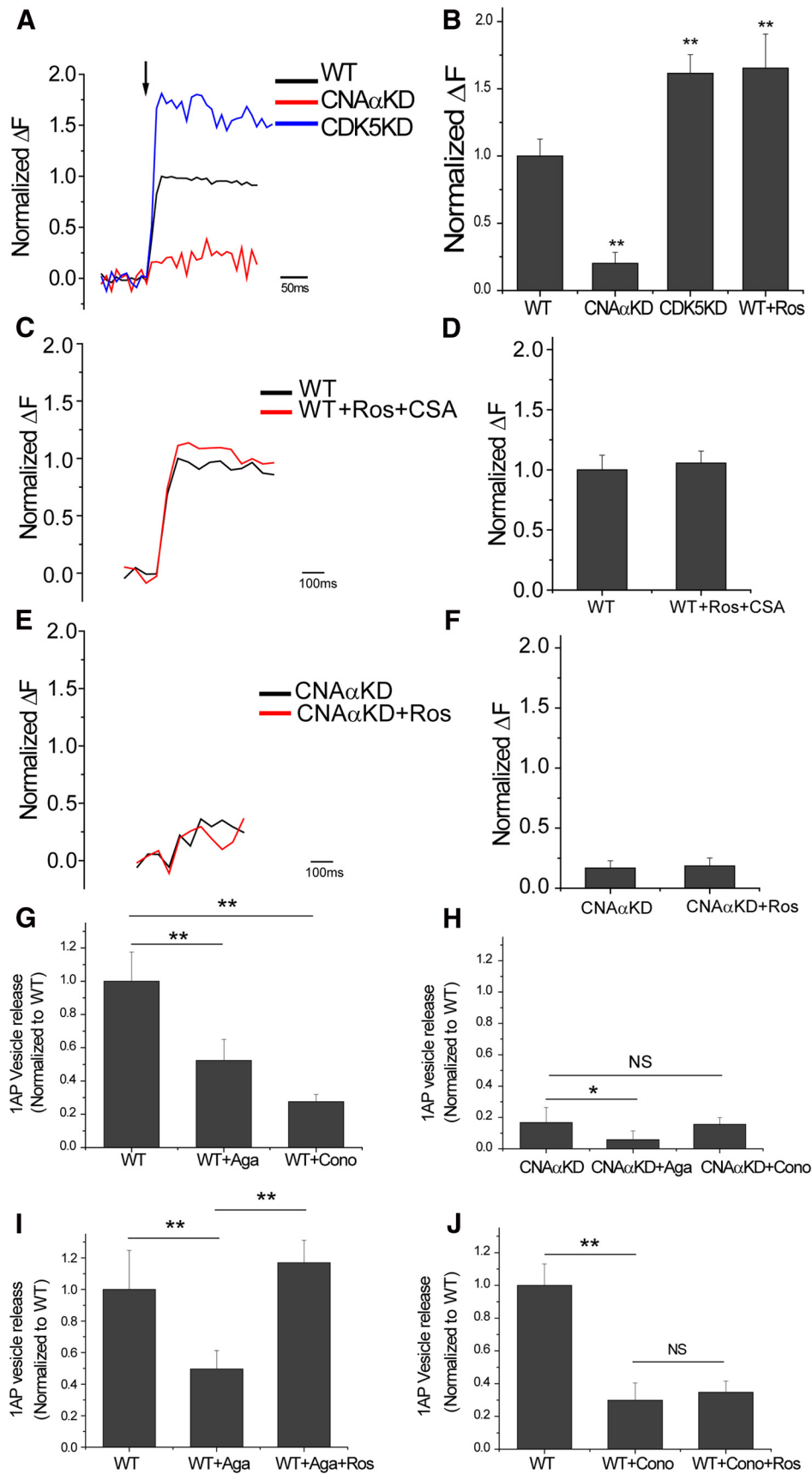


Figure 2. CNA α and CDK5 regulate 1AP-stimulated vesicle release at nerve terminals. **A**, Ensemble average traces of 1AP-stimulated exocytosis reported by vG-pH in WT, CNA α KD, and CDK5KD synapses. **B**, Mean values of 1AP vG-pH response amplitudes normalized to WT in WT, CNA α KD, CDK5KD, and WT neurons treated with roscovitine (Ros). WT_{1AP} = 1.00 \pm 0.12 (n = 20), CNA α KD_{1AP} = 0.23 \pm 0.08 (n = 8), CDK5KD_{1AP} = 1.61 \pm 0.13 (n = 8), and WT + Ros_{1AP} = 1.65 \pm 0.25 (n = 10). **C**, Ensemble average of 1AP-stimulated (Figure legend continues.)

hibitor CSA led to an $\sim 40\%$ drop in Ca $^{2+}$ influx. In nerve terminals lacking CNA α , Ca $^{2+}$ transients were $\sim 50\%$ smaller than controls and were no longer sensitive to CSA (Fig. 3*B,C*). In contrast, acute inhibition of CDK5 by application of roscovitine led to $\sim 30\%$ potentiation of Ca $^{2+}$ influx. Nerve terminals that lacked CDK5 showed Ca $^{2+}$ influx that was $\sim 30\%$ larger than in controls and were insensitive to roscovitine (Fig. 4*D,E*). Although there have been reports of non-CDK5-mediated effects of roscovitine, the equivalence of the impact of the KD of CDK5 and the occlusion of any additional impact by roscovitine argues strongly against this possibility under our recording conditions. Simultaneous blockade of CDK5 and CN using roscovitine and CSA prevented either from modulating AP-driven Ca $^{2+}$ influx (Fig. 3*F*). Similarly, the effect of roscovitine on Ca $^{2+}$ influx was abolished in neurons in which CNA α expression was suppressed previously (Fig. 3*G*). These data all suggest that these two enzymes share a substrate that regulates Ca $^{2+}$ influx through Cav2.2.

Control of exocytosis and Ca $^{2+}$ influx at 1.2 mM external Ca $^{2+}$

In the results described above, we took advantage of the large signal-to-noise ratio available for optical measurements of both Ca $^{2+}$ influx and exocytosis when performing measurements at supraphysiological external Ca $^{2+}$ concentration (4 mM). We previously examined the relationship between Ca $^{2+}$ influx and 1AP-driven exocytosis at nerve terminals (Ariel and Ryan, 2010) and showed that this was well described by a simple generalized Hill equation with a Hill coefficient of ~ 3.4 , in agreement with numerous studies. This nonlinear behavior suggests that the impact of CDK5 and CNA α on exocytosis might differ substantially under more physiological external Ca $^{2+}$ conditions (1.2 mM). As expected, 1AP vG-pH responses were much smaller ($\sim 1/10$) at the lower external calcium concentration compared with that obtained at 4 mM Ca $^{2+}$ (Fig. 4*A*). However, inhibition of CDK5 by application of roscovitine still led to a robust potentiation of release probability (Fig. 4*A*), which now corresponded to an almost fourfold potentiation of 1AP exocytosis (Fig. 4*B*), significantly greater than the $\sim 60\%$ potentiation obtained using 4 mM Ca $^{2+}$. However, measurements of calcium influx using 1.2 mM Ca $^{2+}$ showed that CDK5 inhibition by application of roscovitine led to a similar potentiation of calcium influx ($\sim 28\%$) to that observed at higher external calcium concentration (Fig. 4*C,D*).

←

(Figure legend continued.) exocytosis recorded by vG-pH in WT and WT with Ros and CSA simultaneously. **D**, Mean values of 1AP responses of vG-pH in WT and WT with Ros and CSA simultaneously. WT $_{1AP}$ = 1.00 \pm 0.12, and WT + Ros + CSA $_{1AP}$ = 1.05 \pm 0.09 (n = 9). **E**, Ensemble average of 1AP-stimulated exocytosis recorded by vG-pH in CNA α KD and CNA α KD with Ros. **F**, Mean values of 1AP vG-pH responses in CNA α KD and CNA α KD treated with Ros. CNA α KD $_{1AP}$ = 0.17 \pm 0.06, and CNA α KD + CSA $_{1AP}$ = 0.19 \pm 0.06 (n = 8). **G**, Mean amplitudes of 1AP vG-pH response in WT neurons normalized to control WT condition for ω -agatoxin IVA (Aga) or ω -conotoxin GVIA (Cono) treatments: WT $_{1AP}$ = 1 \pm 0.18 (n = 17), WT + Aga $_{1AP}$ = 0.52 \pm 0.13 (n = 7), and WT + Cono $_{1AP}$ = 0.28 \pm 0.04 (n = 10). **H**, Mean amplitudes of 1AP vG-pH responses in CNA α KD neurons normalized to control WT conditions for ω -agatoxin IVA and ω -conotoxin GVIA treatments: CNA α KDonly $_{1AP}$ = 0.17 \pm 0.09 (n = 16), CNA α KD + Aga $_{1AP}$ = 0.06 \pm 0.06 (n = 10), and CNA α KD + Cono $_{1AP}$ = 0.16 \pm 0.04 (n = 6). **I**, Mean amplitudes of 1AP vG-pH response in WT neurons normalized to WT control condition for Aga + Ros treatments: WT $_{1AP}$ = 1 \pm 0.24 (n = 5), WT + Aga $_{1AP}$ = 0.50 \pm 0.12 (n = 5), and WT + Aga + Ros $_{1AP}$ = 1.17 \pm 0.15 (n = 5). **J**, Mean amplitudes of 1AP vG-pH response in WT neurons normalized to WT control condition for Cono and ω -Cono + Ros treatments: WT $_{1AP}$ = 1 \pm 0.13 (n = 9), WT + Cono $_{1AP}$ = 0.30 \pm 0.1 (n = 9), and WT + Cono + Ros $_{1AP}$ = 0.35 \pm 0.07 (n = 9). * p < 0.05, ** p < 0.01. NS, Not significantly different.

The differences in the level of potentiation obtained for the different external calcium concentrations are well accounted for by the shape of the relationship of calcium influx and exocytosis previously determined in this system (Fig. 4*E*), indicating that impact of CNA α and CDK5 modulation of 1AP-triggered exocytosis is fully accounted for by its impact on Ca $^{2+}$ influx over a range of external calcium concentrations.

CNA α controls Ca $^{2+}$ influx through presynaptic N-type Ca $^{2+}$ channels

Our measurements of calcium influx at single nerve terminals made use of fast recording, high buffer concentrations, and high-affinity probes to ensure the validity of the interpretation that the two counteracting enzymatic activities were controlling calcium influx. We sought to determine whether one could use higher throughput approaches, in particular genetically encoded calcium indicators, to proceed with additional experiments. To this end, we compared 1AP calcium signals using Fluo5F and the genetically encoded calcium indicator GCaMP3 (Tian et al., 2009) as well as the lower-affinity calcium probe MgGreen (Fig. 5). These experiments revealed that, once the nonlinearity of GCaMP3 and been taken into account (Hoppa et al., 2012) (see Materials and Methods), the different probes reported quantitatively identical modulation of 1AP-driven calcium influx by CNA α and CDK5 ablations, respectively.

The data in Figures 2 and 3 imply that CNA α and CDK5 specifically act by controlling AP-driven calcium influx through Cav2.2 channels at synapses. We tested this hypothesis by measuring calcium influx at synapses using GCaMP3 after blockade by Cav2.1 or Cav2.2 while simultaneously manipulating CNA α or CDK5 activity. At synapses, application of the specific Cav2.1 blocker ω -agatoxin IVA led to an $\sim 20\%$ inhibition of 1AP-driven Ca $^{2+}$ influx, whereas application of the Cav2.2 blocker ω -conotoxin GVIA suppressed $\sim 50\%$ of the total Ca $^{2+}$ influx (Fig. 6*A*). In neurons in which CNA α expression has been suppressed, only agatoxin, but not conotoxin, could further reduce Ca $^{2+}$ influx. These data indicate that no Cav2.2 function persists in the absence of CNA α activity (Fig. 5*B*). Similarly application of roscovitine to block CDK5 activity showed full potentiation even in the absence of Ca $^{2+}$ influx through Cav2.1 (Fig. 6*C*) but showed no effect when Cav2.2 channels were blocked (Fig. 6*C,D*). We wondered whether the ability of CDK5 and CNA α to control calcium influx via Cav2.2 was restricted to nerve terminals. To examine this, we adapted our protocols to examine calcium influx at cell somas (Fig. 6*E-H*). Although we found that the proportional contributions to 1AP-triggered somatic Ca $^{2+}$ influx by Cav2.1 and Cav2.2 was different from that at nerve terminals (Fig. 6*E*), the relative modulation of calcium influx through these VGCCs via CDK5 and CNA α was similar to that observed presynaptically (Fig. 6*F-H*). Collectively, we conclude that the modulation of AP-triggered Ca $^{2+}$ influx by CNA α and CDK5 is restricted to Cav2.2 VGCCs.

The balance of CNA α and CDK5 eliminates Ca $^{2+}$ influx at some boutons

We showed previously that subsets of synaptic boutons are in a functionally silent state, failing to show any exocytic response, even during robust AP stimulation. Our experiments revealed that acute blockade of CDK5 activity would unmask a large fraction of this silent population (Kim and Ryan, 2010). Therefore, we wondered whether this silencing was attributable to an absence of AP-triggered Ca $^{2+}$ entry or other downstream steps related to exocytosis. To examine this, we made use of synaptically

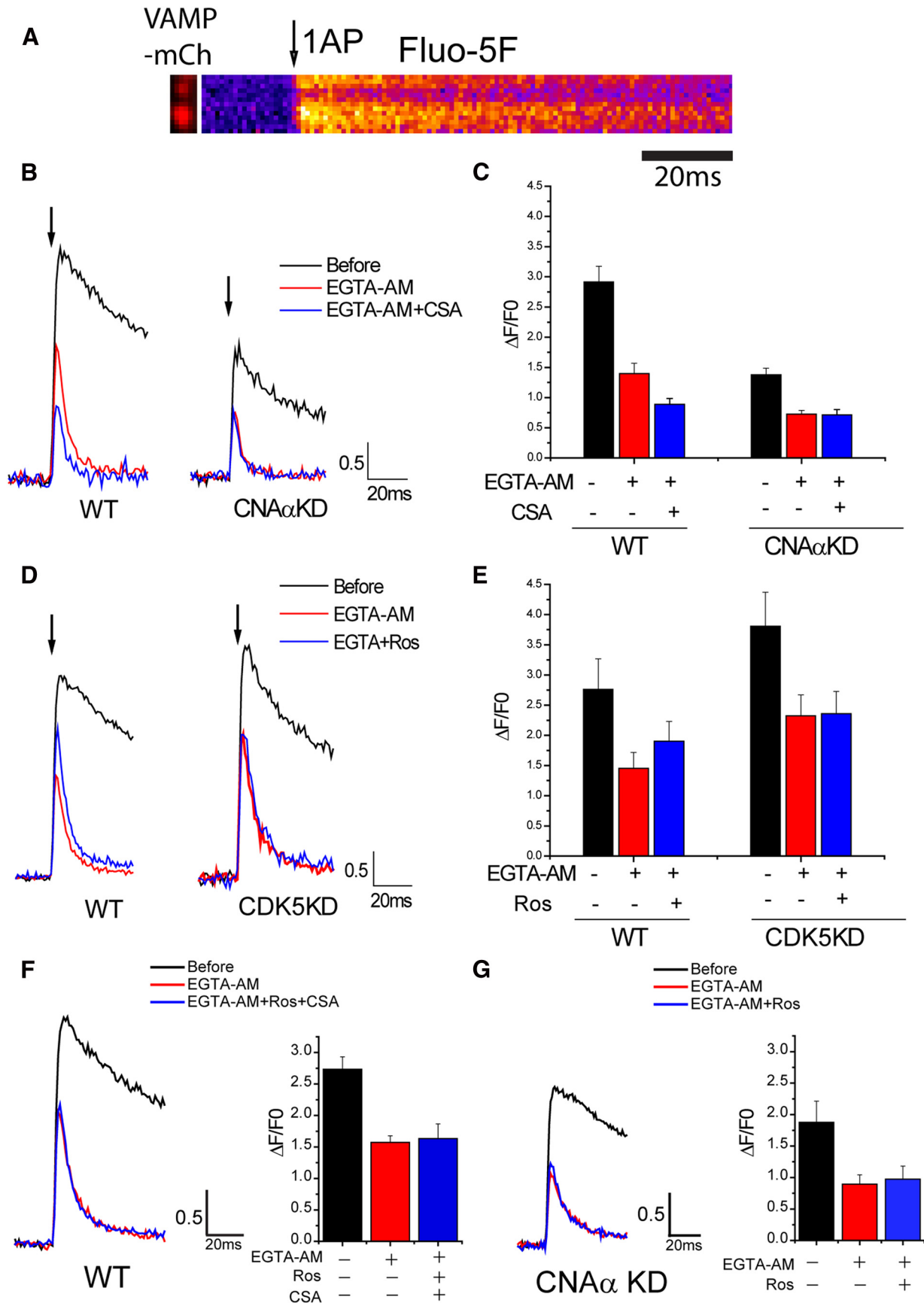


Figure 3. CNA α and CDK5 regulate AP-stimulated Ca²⁺ influx at nerve terminals. **A**, Representative images of VAMP2-mCh and its corresponding Fluo5F kymograph image for 1AP stimulation in WT. **B**, Representative 1AP Fluo5F traces before (black) and after (red) EGTA-AM with CSA (blue) in WT (left) and CNA α KD (right) neurons. Arrow indicates 1AP point. **C**, Mean value of Fluo5F 1AP response amplitudes before and after EGTA-AM with/without CSA in WT and CNA α KD neurons: WT_{Before 1AP} = 2.92 ± 0.26, WT_{EGTA-AM 1AP} = 1.40 ± 0.17, (Figure legend continues.)

targeted GCaMP3 (synaptophysin–GCaMP3) (Tian et al., 2009). We examined IAP responses averaged over many trials (10–15) across populations of synapses expressing this reporter, followed by application of the Ca²⁺ ionophore ionomycin, which elevates Ca²⁺ in all synapses (Fig. 7A). These experiments revealed that, as with exocytosis, a fraction of nerve terminals fail to show any Ca²⁺ signal in response to IAP stimulation (Fig. 7A,B) but were unmasked by blockade of CDK5 activity with roscovitine. Conversely, some synapses that showed a robust AP-triggered Ca²⁺ signal under control conditions could be completely silenced after inhibition of CN with CSA (Fig. 7A,B). On average, we found that ~10–15% of all boutons sampled failed to show any Ca²⁺ signal and that approximately half of these were unmasked with CDK5 blockade, whereas greater than ~35% of boutons became silent after CN inhibition (Fig. 7C). Similar results were obtained using MgGreen-AM loading of VAMP2–mCh-expressing nerve terminals (Fig. 7D). These data imply that a fraction of nerve terminals rely solely on Cav2.2 because they were silent originally and converted to a functional state by CDK5 inhibition. We tested this hypothesis by examining what fraction of boutons are silent after addition of conotoxin and a combination of conotoxin and the CDK5 inhibitor roscovitine. These experiments showed that the proportion of silent boutons increases significantly after conotoxin treatment and that these boutons are now refractory to CDK5 blockade (Fig. 7E). In contrast, although the fraction of silent boutons increases after agatoxin treatment, this fraction decreases after CDK5 blockade (Fig. 7E). Thus, the balance of activity between CNA α and CDK5 exerts a potent influence on VGCC function, which results in a complete silencing at the level of some nerve terminals, ones that contained primarily Cav2.2 channels.

Discussion

We recently demonstrated that CDK5 and CN activities control what fraction of synaptic vesicles at nerve terminals partition into recycling or resting synaptic vesicle pools. These experiments revealed that these enzymes additionally control AP-triggered exocytosis efficiency for those vesicles in the recycling pool. The experiments we present here demonstrated that these enzymes are constantly in balance to control Ca²⁺ influx triggered by AP stimulation at synapses and have revealed a potent new form of synaptic transmission modulation that operates down to the IAP level. Neurotransmitter release can in principle be controlled at several levels. Given the cooperativity of Ca²⁺ action in exocytosis, modulation of Ca²⁺ influx at the active zone of presynaptic terminals is a potent mechanism to influence neurotransmitter

release and is considered one of the main mechanisms by which presynaptic metabotropic modulation is achieved (Agler et al., 2005; Tedford and Zamponi, 2006). We tested the hypothesis that CDK5 and CN were controlling the efficacy of AP-triggered exocytosis through modulation of Ca²⁺ influx by measuring Ca²⁺ influx at nerve terminals in which the activity of these enzymes had been curtailed by pharmacological or shRNA-based KD. The pharmacological experiments showed that these enzyme functions can control Ca²⁺ entry on relatively short timescales (minutes). Furthermore, the impact of the pharmacological blockade on calcium influx was very similar to that of the KDs, and the KDs were insensitive to additional pharmacological inhibition verifying the specificity of the drug action. Roscovitine in particular had been implicated in directly modifying VGCC function independent of CDK5 (Yan et al., 2002). However, these studies examined roscovitine effects only in the absence of one of the cyclins of CDK5, not in the absence of CDK5. Our results demonstrate that an off-target modulation of VGCCs by roscovitine is unlikely because ablation of CDK5 fully mimics the effect of roscovitine on Cav2.2 and occludes additional modulation by this drug.

Homeostatic synaptic plasticity is a well-established control mechanism for synaptic transmission in neural circuits (Davis, 2006), and both presynaptic and postsynaptic efficacy can be retuned in response to chronic changes of neural activity via different molecular mechanisms (Ehlers, 2003; Müller et al., 2011). Previously, we showed that long-term suppression of neuronal activity caused loss of CDK5 activity and by doing so increases the size of the releasable vesicle pool (Kim and Ryan, 2010). Recently, Zhao et al. (2011) reported that chronic neuronal inhibition potentiated presynaptic Ca²⁺ influx and release probability. The results we show here, along with our previous observation, suggest that chronic neuronal activity, through control of CDK5 levels, modulates AP-driven Ca²⁺ influx at nerve terminals.

Our quantitative measurements of the control of IAP-triggered Ca²⁺ entry and exocytosis by CNA α and CDK5 inhibition are in excellent agreement with previously published measurements of how vesicle fusion probability varies with changes in Ca²⁺ influx (Ariel and Ryan, 2010). Thus, one can accurately attribute all of the effects of CNA α or CDK5 modulation of IAP exocytosis to their impact on Ca²⁺ influx (Fig. 4E). Our previous examination of the functions of these enzymes in nerve terminals revealed that they control partitioning of vesicles into resting and recycling pools (Kim and Ryan, 2010). This activity we believe is separate from the control of Ca²⁺ influx, because explicitly changing Ca²⁺ influx does not change resting and recycling pool sizes (Fernandez-Alfonso and Ryan, 2008). Furthermore, application of conotoxin that eliminates Cav2.2 function does not affect recycling vesicle pool sizes nor does it interfere with ability to increase recycling vesicle pools by blocking CDK5 (data not shown). However, given that CN is modulated by intracellular Ca²⁺, the potent control of Ca²⁺ entry by CN demonstrates that CN acts in a positive feedback loop that could potentially lead to all-or-none-type behavior in synaptic performance.

Our analysis of the CN isoform specificity led to a very surprising finding. CN function has been well documented across many biological systems and is most famously the target of therapeutic immunosuppression with CSA or FK506. These drugs work by forming a ternary complex with CN (CNA and CNB) and either cyclophilin (for CSA) or an immunophilin (for FK506). We found that both α and β isoforms of CNA are present in nerve terminals, but only the α isoform appears to function in

←

(Figure legend continued.) WT_{EGTA-AM + CSA IAP} = 0.89 ± 0.10 (n = 8), CNA α KD_{Before IAP} = 1.38 ± 0.11, CNA α KD_{EGTA-AM IAP} = 0.73 ± 0.06, and CNA α KD_{EGTA-AM + CSA IAP} = 0.71 ± 0.09 (n = 9). **D**, Representative IAP Fluo5F traces before (black) and after (red) EGTA-AM with roscovitine (Ros) (blue) in WT (left) and CDK5KD (right) neurons. Arrow indicates IAP point. **E**, Mean value of Fluo5F IAP response amplitudes before and after EGTA-AM with/without roscovitine in WT and CDK5KD neurons: WT_{Before IAP} = 2.76 ± 0.51, WT_{EGTA-AM IAP} = 1.45 ± 0.26, WT_{EGTA-AM + Ros IAP} = 1.90 ± 0.33 (n = 7), CDK5KD_{Before IAP} = 3.81 ± 0.56, CDK5KD_{EGTA-AM IAP} = 2.32 ± 0.35, and CDK5KD_{EGTA-AM + Ros IAP} = 2.36 ± 0.37 (n = 8). **F**, Left, Representative IAP Fluo5F traces before (black) and after (red) EGTA-AM with Ros and CSA (blue) in WT neurons. Right, Mean value of Fluo5F IAP response amplitudes before and after EGTA-AM with/without Ros and CSA in WT neurons: WT_{Before IAP} = 2.73 ± 0.19, WT_{EGTA-AM IAP} = 1.57 ± 0.10, and WT_{EGTA-AM + Ros + CSA IAP} = 1.63 ± 0.23 (n = 5). **G**, Left, Representative IAP Fluo5F traces before (black) and after (red) EGTA-AM with Ros (blue) in CNA α KD neurons. Right, Mean value of Fluo5F IAP response amplitudes before and after EGTA-AM with/without Ros in CNA α KD neurons: CNA α KD_{Before IAP} = 1.87 ± 0.33, CNA α KD_{EGTA-AM IAP} = 0.89 ± 0.14, and CNA α KD_{EGTA-AM + Ros IAP} = 0.97 ± 0.20. (n = 5).

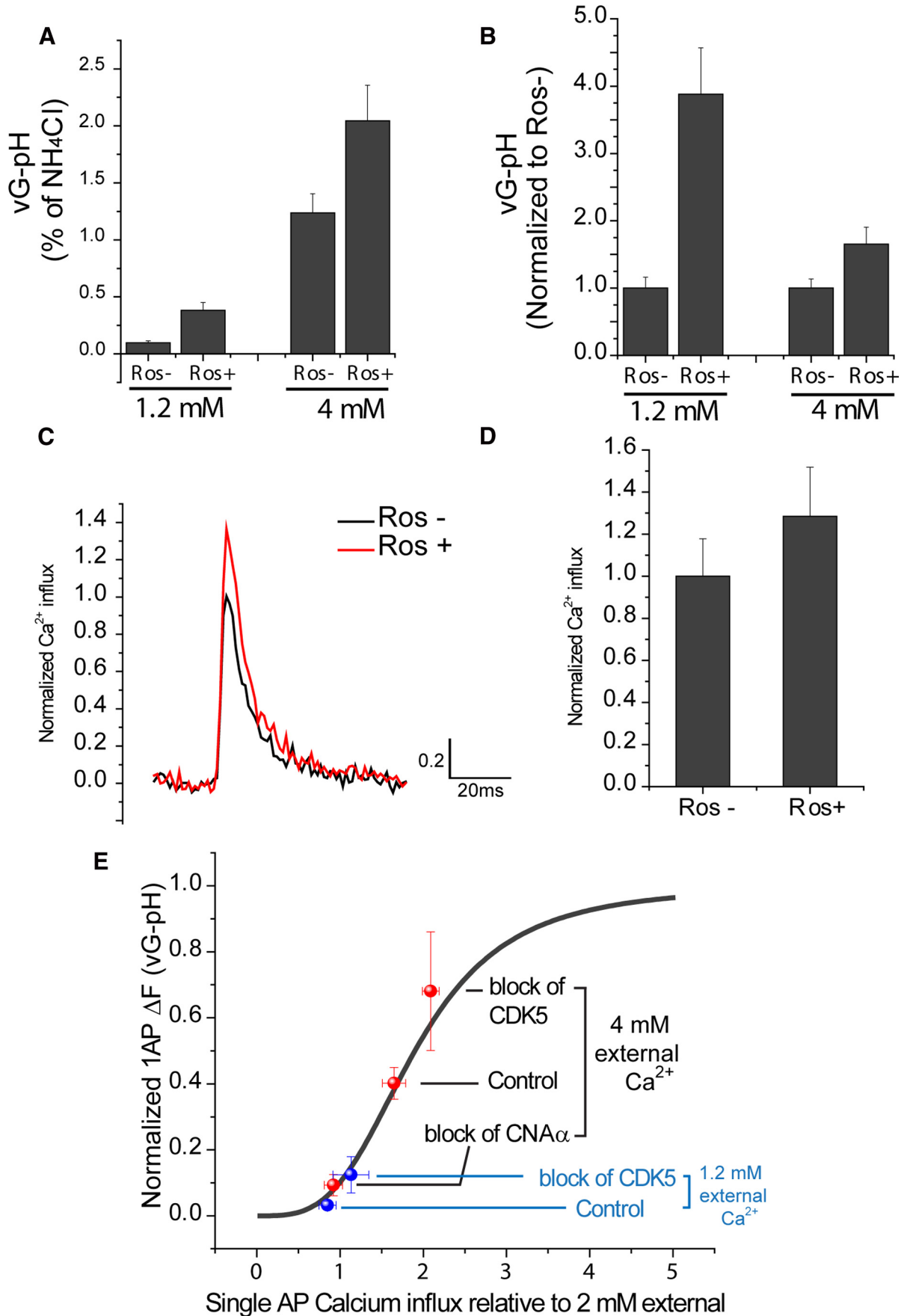


Figure 4. Manipulation of exocytosis and Ca²⁺ influx at 1.2 mM external Ca²⁺. **A**, Comparison of mean values of 1AP-driven exocytosis reported by vG-pH at 1.2 and 4 mM external Ca²⁺ with/without roscovitine (Ros) (expressed as percentage of NH₄Cl): 1.2 mM_{Ros⁻} = 0.098 ± 0.016, 1.2 mM_{Ros⁺} = 0.382 ± 0.068 (n = 15), (Figure legend continues.)

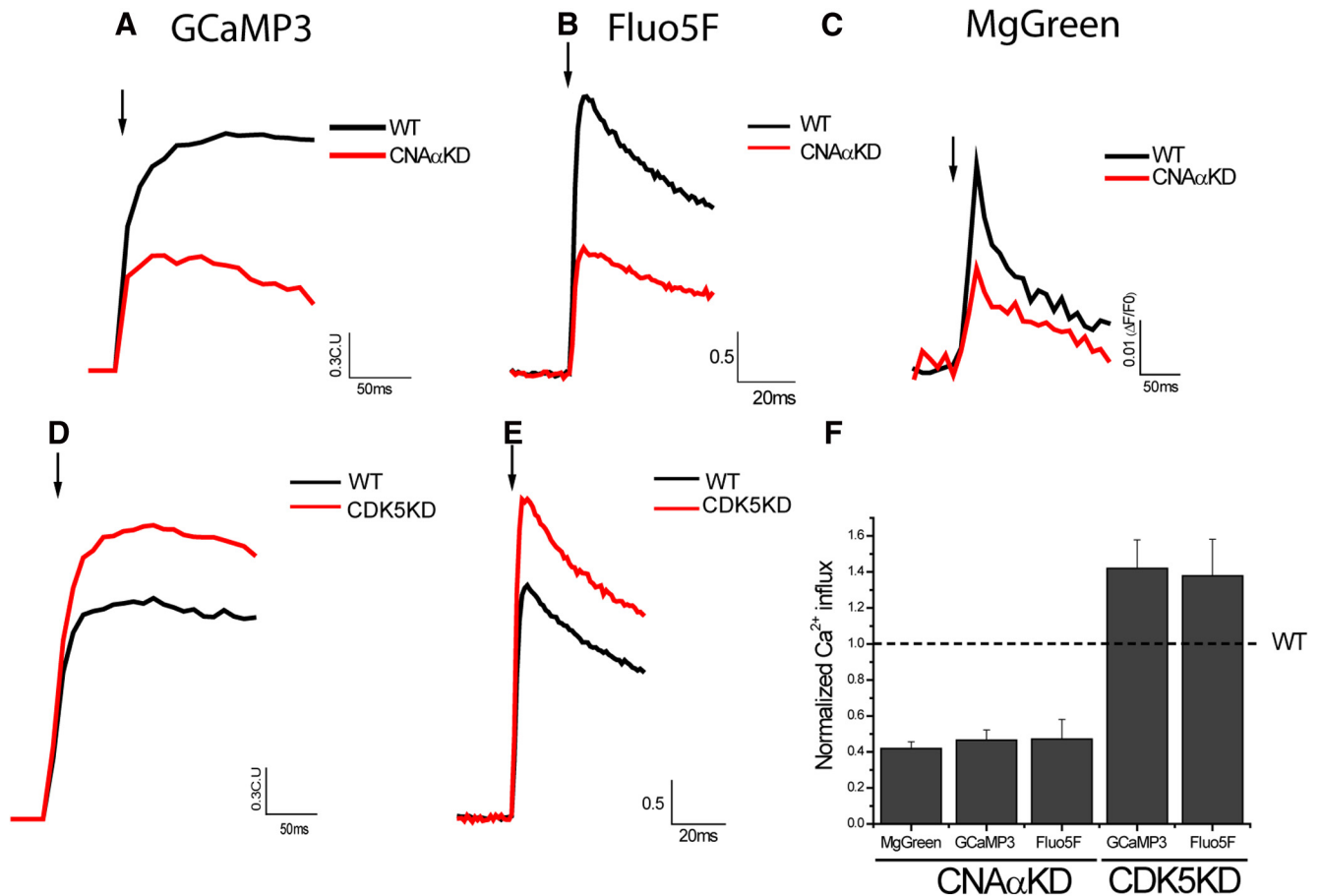


Figure 5. Comparison of 1AP-driven Ca^{2+} influx with three different calcium indicators: GCaMP3, Fluo5F, and MgGreen. **A–C**, Ensemble average traces of 1AP-triggered Ca^{2+} influx responses of linearized Physin–GCaMP3 (**A**), Fluo5F (**B**), or MgGreen (**C**) in VAMP–mCh-positive puncta in WT (black) and CNA α KD (red) neurons. **D, E**, Ensemble average traces of 1AP-triggered Ca^{2+} influx responses of linearized Physin–GCaMP3 (**D**) or Fluo5F (**E**) in VAMP–mCh-positive puncta in WT (black) and CDK5KD (red) neurons. **F**, Normalized mean values of 1AP-triggered Ca^{2+} influx. $\text{GCaMP3}_{\text{CNA}\alpha\text{KD}}^{\text{1AP}} = 0.42 \pm 0.04$ ($n = 7$), $\text{Fluo5F}_{\text{CNA}\alpha\text{KD}}^{\text{1AP}} = 0.47 \pm 0.06$ ($n = 9$), $\text{MgGreen}_{\text{CNA}\alpha\text{KD}}^{\text{1AP}} = 0.47 \pm 0.11$ ($n = 6$), $\text{GCaMP3}_{\text{CDK5KD}}^{\text{1AP}} = 1.42 \pm 0.16$ ($n = 10$), and $\text{Fluo5F}_{\text{CNA}\alpha\text{KD}}^{\text{1AP}} = 1.38 \pm 0.20$ ($n = 8$).

the control of VGCC-mediated Ca^{2+} influx: ablation of CNA α expression and not CNA β led to suppression of Ca^{2+} influx, and ablation of CNA α expression also eliminated sensitivity of Ca^{2+} influx to CSA. Thus, these isoforms are not redundant and appear to serve distinct functions. Previously, these two CNA isoforms have been reported to serve similar functions in different brain regions based on knock-outs of the individual genes (Sun et al., 2010). Although no measure of VGCC activity in these knock-

outs was reported, it is possible that compensatory upregulation of VGCCs was occurring given that genetic ablation of specific VGCC pore-forming subunits is known to lead to direct upregulation of alternate pore-forming subunits (Inchauspe et al., 2004).

At nerve terminals, the most prominent known targets of CDK5 and CN are endocytic proteins, such as dynamin, amphiphysin, and synaptojanin, named dephosphins, so named because they become dephosphorylated by CN during activity (Cousin and Robinson, 2001). The physiological role of this dephosphorylation in controlling endocytosis has been difficult to determine precisely, although the biochemical consequence of the dephosphorylation of dynamin are better understood (Anggono et al., 2006). In retrospect, a difficulty associated with studies using inhibition of these enzymes was likely the perturbation of Ca^{2+} flux, which in turn will have pleiotropic effects beyond controlling CN.

Although N-type channels were recently demonstrated to be substrates for CDK5-mediated phosphorylation *in vitro* (Su et al., 2012), our results come to opposite conclusions than would be predicted by that work regarding how CN and CDK5 would in turn influence presynaptic function. The reasons for these differences are unclear. The most parsimonious explanation for the discrepancy is that, although CDK5 may be capable of phosphorylating the previously identified sites, in the physiological con-

←

(Figure legend continued.) $4 \text{ mM}_{\text{Ros-}} = 1.23 \pm 0.16$, and $4 \text{ mM}_{\text{Ros+}} = 2.04 \pm 0.3$ ($n = 10$). **B**, Normalized response to exocytosis without Ros (Ros $^-$) at 1.2 or 4 mM Ca^{2+} : $1.2 \text{ mM}_{\text{Ros-}} = 1.00 \pm 0.16$, $1.2 \text{ mM}_{\text{Ros+}} = 3.88 \pm 0.68$ ($n = 15$), $4 \text{ mM}_{\text{Ros-}} = 1.00 \pm 0.14$, and $4 \text{ mM}_{\text{Ros+}} = 1.65 \pm 0.25$ ($n = 10$). **C**, Representative trace of Fluo5F to 1AP at 1.2 mM external Ca^{2+} with/without Ros in WT synapses. **D**, Normalized mean values of 1AP-driven Fluo5F response amplitudes with/without Ros at 1.2 mM external Ca^{2+} . $1.2 \text{ mM}_{\text{Ros-}} = 1.00 \pm 0.17$, and $1.2 \text{ mM}_{\text{Ros+}} = 1.28 \pm 0.23$ ($n = 7$). **E**, Comparison of response modulation by blocking either CNA α or CDK5 with the known Ca^{2+} dependence of exocytosis in this system. This curve has a Hill coefficient of 3.4 and is normalized along the x-axis to the Ca^{2+} influx obtained using 2 mM external CaCl_2 (Ariel and Ryan, 2010). For comparison, we mapped the results of the experiments with CNA α and CDK5 manipulations on exocytosis and Ca^{2+} influx relative to the controls [measured at 2 different external Ca^{2+} concentrations, 1.2 mM (blue) and 4 mM (red), in this study]. Value of 1.2 mM Ca^{2+} on x-axis is calculated as relative value from 4 mM Ca^{2+} value. The data appear to fall along the originally mapped Ca^{2+} influx curve, suggesting that the full effect of CNA α and CDK5 inhibition on exocytosis can be attributed to changes in Ca^{2+} influx.

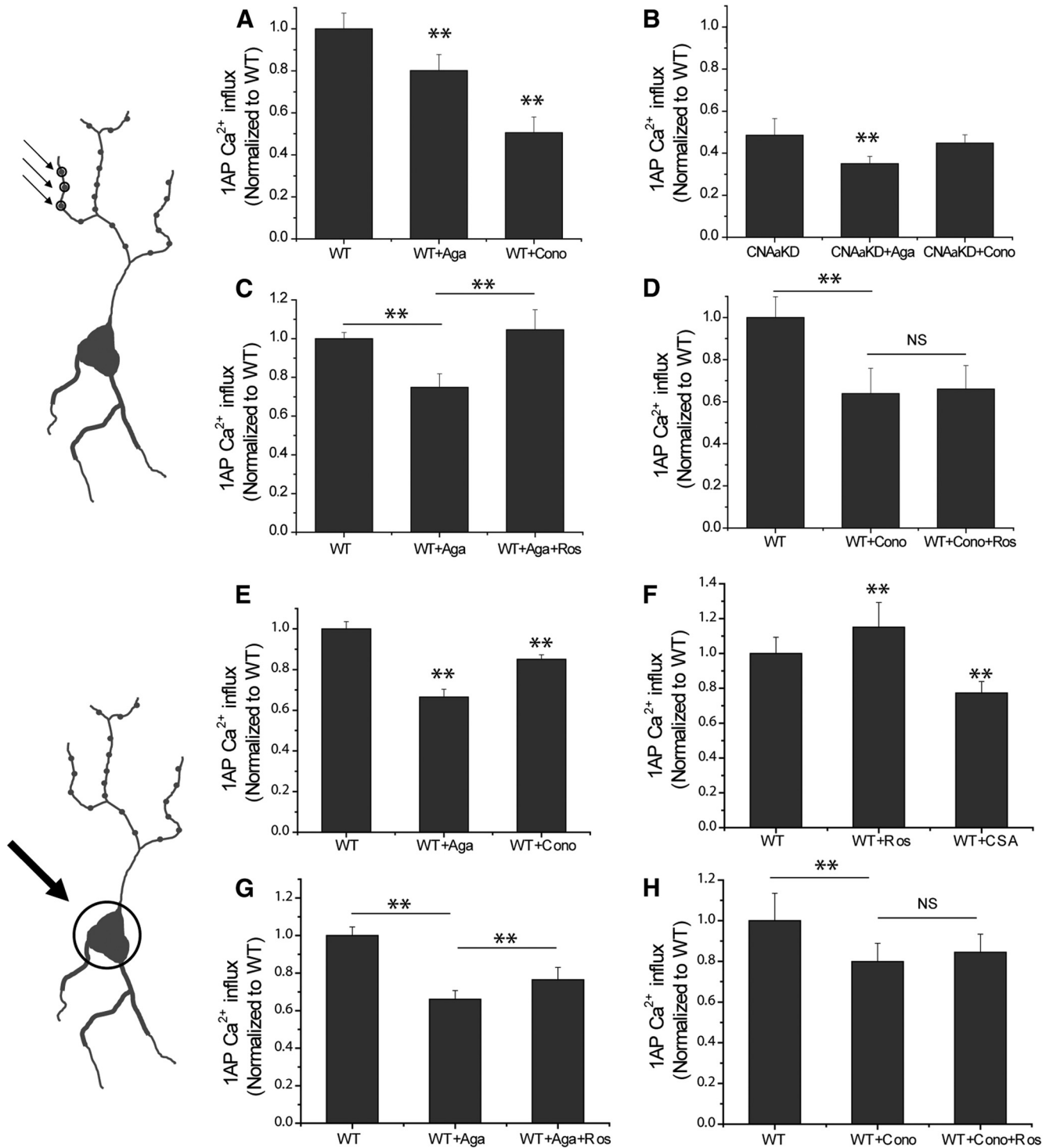


Figure 6. CNA α and CDK5 regulate N-type but not P/Q-type Ca²⁺ channels at hippocampal synapses and soma. **A–D**, Measurement of Ca²⁺ influx with synaptophysin–GCaMP3 at presynaptic terminal with/without ω -agatoxin IVA or ω -conotoxin GVIA in WT and CNA α KD neurons. **A**, Mean linearized 1AP GCaMP3 response amplitudes at boutons in WT neurons normalized to control condition for ω -agatoxin IVA (Aga) or ω -conotoxin GVIA (Cono) treatments: WT_{boutons 1AP} = 1.00 ± 0.07 (*n* = 24), WT + Aga_{boutons 1AP} = 0.80 ± 0.07 (*n* = 16), and WT + Cono_{boutons 1AP} = 0.50 ± 0.07 (*n* = 8). **B**, Mean linearized 1AP GCaMP3 responses in CNA α KD neurons normalized to control WT conditions for Aga and Cono treatments: CNA α KD_{boutons 1AP} = 0.49 ± 0.08 (*n* = 14), CNA α KD + Aga_{boutons 1AP} = 0.35 ± 0.03 (*n* = 6), and CNA α KD + Cono_{boutons 1AP} = 0.44 ± 0.04 (*n* = 8). **C**, Mean linearized 1AP GCaMP3 response amplitudes in WT neurons normalized to WT control condition for Aga and Aga + roscovitine (Ros) treatments: WT_{boutons 1AP} = 1.00 ± 0.03, WT + Aga_{boutons 1AP} = 0.75 ± 0.07, and WT + Aga + Ros_{boutons 1AP} = 1.05 ± 0.10 (*n* = 7). **D**, Mean linearized 1AP GCaMP3 response amplitudes in WT neurons normalized to WT control condition for ω -conotoxin GVIA (Cono) and Cono + Ros treatments: WT_{boutons 1AP} = 1.00 ± 0.10, WT + Cono_{boutons 1AP} = 0.63 ± 0.12, and WT + Cono + Ros_{boutons 1AP} = 0.66 ± 0.11 (*n* = 7). **E–H**, Measurement of somatic Ca²⁺ influx with Fluo5F with/without ω -agatoxin IVA or ω -conotoxin GVIA and roscovitine in WT neurons. **E**, Mean 1AP response amplitudes of Ca²⁺ influx at cell somas in WT neurons normalized to control condition for Aga or Cono treatments: WT_{soma 1AP} = 1.00 ± 0.03 (*n* = 23), WT + Aga_{soma 1AP} = 0.66 ± 0.03 (*n* = 9), and WT + Cono_{soma 1AP} = 0.85 ± 0.02 (*n* = 14). **F**, Mean 1AP response amplitudes of Ca²⁺ influx at cell body with/without roscovitine or CSA: WT_{soma 1AP} = 1.00 ± 0.09 (*n* = 19), WT + Ros_{soma 1AP} = 1.15 ± 0.14 (*n* = 9), and WT + CSA_{soma 1AP} = 0.77 ± 0.06 (*n* = 10). **G**, Mean 1AP response amplitudes of Ca²⁺ influx at cell body with Aga and Aga + Ros treatments: WT_{soma 1AP} = 1.00 ± 0.04, WT + Aga_{soma 1AP} = 0.66 ± 0.04, and WT + Aga + Ros_{soma 1AP} = 0.76 ± 0.06 (*n* = 7). **H**, Mean 1AP response amplitudes of Ca²⁺ influx at cell body with Cono and Cono + Ros treatments: WT_{soma 1AP} = 1.00 ± 0.13, WT + Cono_{soma 1AP} = 0.79 ± 0.09, and WT + Cono + Ros_{soma 1AP} = 0.84 ± 0.08. (*n* = 6). ***p* < 0.01. NS, Not significantly different.

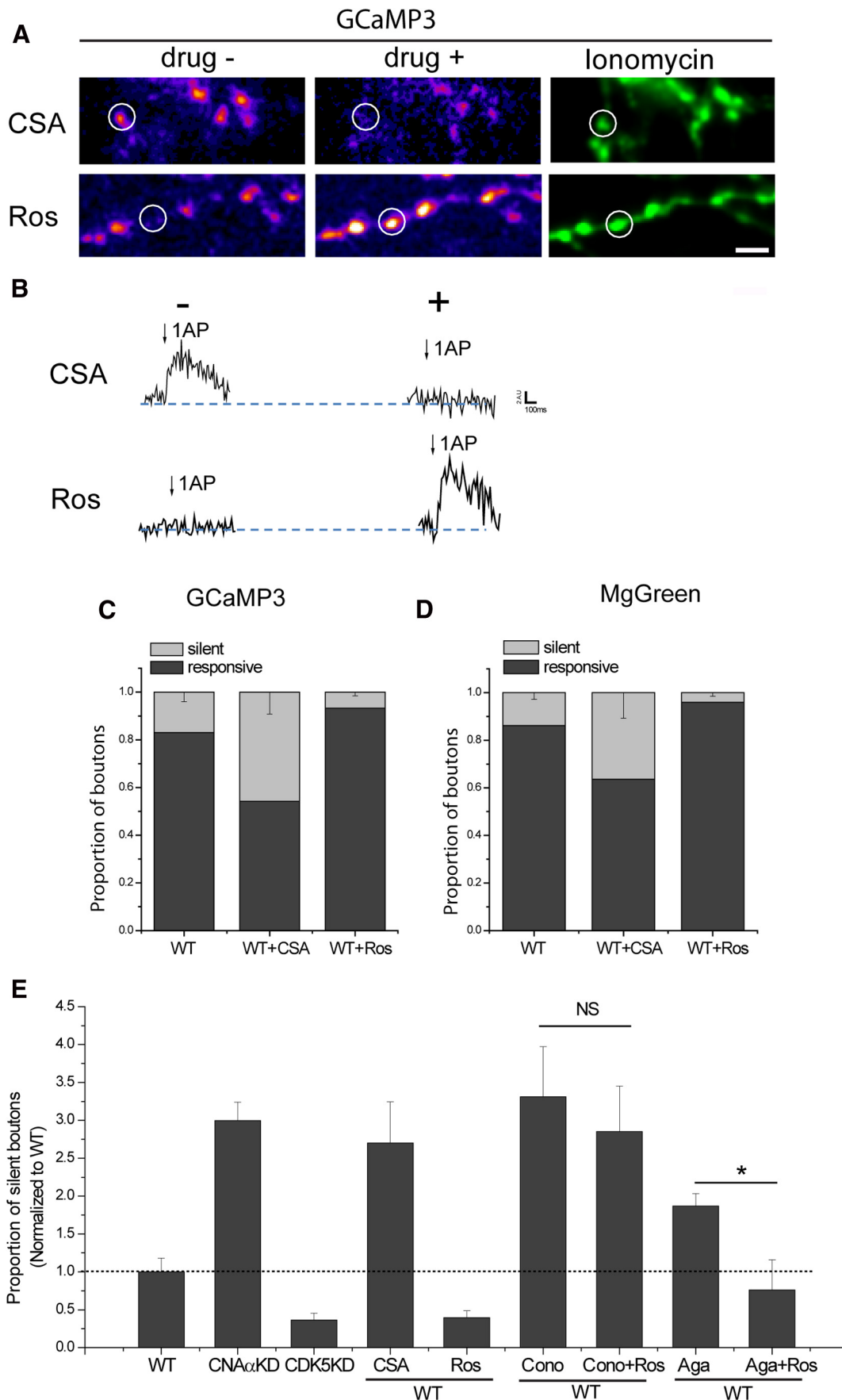


Figure 7. CNA α and CDK5 gate silent presynaptic boutons by controlling Ca²⁺ influx. **A**, Representative 1AP GCaMP3 difference image (ΔF_{1AP}) in WT neurons in the absence or presence of CSA (top) or roscovitine (Ros) (bottom). Ionomycin treatment (right) reveals all presynaptic boutons. White circles indicate boutons that were silenced after (*Figure legend continues.*)

text, they might be overridden by other factors controlled by CDK5 and CN that also influence calcium influx. The functional expression of VGCCs at nerve terminals requires several steps, including a chaperone-mediated exit from the endoplasmic reticulum, axonal transport, and trafficking from a local presynaptic endosome to the presynaptic plasma membrane. We recently demonstrated that successful integration of VGCCs into active zones to drive exocytosis requires the integrity and participation of the $\alpha\delta$ subunit (Hoppa et al., 2012). In the work by Su et al. (2012), the evidence for the role of the eight identified serines in Cav2.2 in synaptic function was based on a loss of function driven by mutating these sites to alanine. If in the context of the nerve terminal these sites are not normally substrates for CDK5 and if mutations at such sites prevented correct trafficking to the active zone, it would have simply led to a loss of synapse function as reported. However, the previous work did not examine the impact of modulation of synaptic function by CDK5 or CN. In contrast, the work we present here suggests that, *in situ*, other CDK5 phosphorylation sites (either on Cav2.2 or another protein) dominate in control of Cav2.2 function.

Our studies demonstrated that, *in situ*, VGCCs are tightly controlled by the enzymatic activities of CN and CDK5 and that these enzymes set the “tone” of Cav2.2 function. Therefore, Cav2.2 channels act as key integrators of these two opposing enzymatic activities. At some synapses, this leads to complete silencing of presynaptic exocytosis. The switch-like behavior of CNA α /CDK5 modulation of calcium entry in a subset of synapses may represent an arbitrary signal-to-noise-driven cutoff of the definition of “silent.” However, the signals were based on robust averaging of ~ 15 trials imposing a generous 1 SD over baseline noise cutoff. However, given the nonlinear coupling of calcium influx and exocytosis, it does provide a good explanation for the switch-like behavior of CNA α /CDK5 modulation of exocytosis seen previously (Kim and Ryan, 2010).

The full range of control of Cav2.2 by these enzymes results in profound impact on synaptic function, corresponding to an approximately sevenfold change in exocytosis. The ubiquitous presence of these enzymes through the brain and the essential role that Ca²⁺ influx plays in controlling synaptic transmission suggest that this pathway likely serves as an important modulator of synaptic transmission throughout the CNS. One of the important areas for future studies will be to understand how CDK5 itself is

modulated either directly or by modifications of its known activating cyclins.

References

- Agler HL, Evans J, Tay LH, Anderson MJ, Colecraft HM, Yue DT (2005) G protein-gated inhibitory module of N-type (ca(v)2.2) Ca²⁺ channels. *Neuron* 46:891–904. [CrossRef Medline](#)
- Anggono V, Smillie KJ, Graham ME, Valova VA, Cousin MA, Robinson PJ (2006) Syndapin I is the phosphorylation-regulated dynamin I partner in synaptic vesicle endocytosis. *Nat Neurosci* 9:752–760. [CrossRef Medline](#)
- Ariel P, Ryan TA (2010) Optical mapping of release properties in synapses. *Front Neural Circuits* 4:pii.18. [CrossRef Medline](#)
- Ariel P, Hoppa MB, Ryan TA (2012) Intrinsic variability in Pv, RRP size, Ca²⁺ channel repertoire, and presynaptic potentiation in individual synaptic boutons. *Front Synaptic Neurosci* 4:9. [CrossRef Medline](#)
- Bibb JA, Snyder GL, Nishi A, Yan Z, Meijer L, Fienberg AA, Tsai LH, Kwon YT, Girault JA, Czernik AJ, Hagan RL, Hemmings HC Jr, Nairn AC, Greengard P (1999) Phosphorylation of DARPP-32 by Cdk5 modulates dopamine signalling in neurons. *Nature* 402:669–671. [CrossRef Medline](#)
- Cousin MA, Robinson PJ (2001) The dephosphins: dephosphorylation by calcineurin triggers synaptic vesicle endocytosis. *Trends Neurosci* 24:659–665. [CrossRef Medline](#)
- Cruz JC, Tsai LH (2004) Cdk5 deregulation in the pathogenesis of Alzheimer's disease. *Trends Mol Med* 10:452–458. [CrossRef Medline](#)
- Davis GW (2006) Homeostatic control of neural activity: from phenomenology to molecular design. *Annu Rev Neurosci* 29:307–323. [CrossRef Medline](#)
- Dhavan R, Tsai LH (2001) A decade of CDK5. *Nat Rev Mol Cell Biol* 2:749–759. [CrossRef Medline](#)
- Ehlers MD (2003) Activity level controls postsynaptic composition and signaling via the ubiquitin-proteasome system. *Nat Neurosci* 6:231–242. [CrossRef Medline](#)
- Fernandez-Alfonso T, Ryan TA (2008) A heterogeneous “resting” pool of synaptic vesicles that is dynamically interchanged across boutons in mammalian CNS synapses. *Brain Cell Biol* 36:87–100. [CrossRef Medline](#)
- Gupta A, Tsai LH (2003) Cyclin-dependent kinase 5 and neuronal migration in the neocortex. *Neurosignals* 12:173–179. [CrossRef Medline](#)
- Hoppa MB, Lana B, Margas W, Dolphin AC, Ryan TA (2012) $\alpha\delta$ expression sets presynaptic calcium channel abundance and release probability. *Nature* 486:122–125. [CrossRef Medline](#)
- Inchauspe CG, Martini FJ, Forsythe ID, Uchitel OD (2004) Functional compensation of P/Q by N-type channels blocks short-term plasticity at the calyx of held presynaptic terminal. *J Neurosci* 24:10379–10383. [CrossRef Medline](#)
- Kim SH, Ryan TA (2009) Synaptic vesicle recycling at CNS synapses without AP-2. *J Neurosci* 29:3865–3874. [CrossRef Medline](#)
- Kim SH, Ryan TA (2010) CDK5 serves as a major control point in neurotransmitter release. *Neuron* 67:797–809. [CrossRef Medline](#)
- Klee CB, Ren H, Wang X (1998) Regulation of the calmodulin-stimulated protein phosphatase, calcineurin. *J Biol Chem* 273:13367–13370. [CrossRef Medline](#)
- Kwon YT, Tsai LH (2000) The role of the p35/cdk5 kinase in cortical development. *Results Probl Cell Differ* 30:241–253. [CrossRef Medline](#)
- Malleret G, Haditsch U, Genoux D, Jones MW, Bliss TV, Vanhoose AM, Weitlauf C, Kandel ER, Winder DG, Mansuy IM (2001) Inducible and reversible enhancement of learning, memory, and long-term potentiation by genetic inhibition of calcineurin. *Cell* 104:675–686. [CrossRef Medline](#)
- Meijer L, Borgne A, Mulner O, Chong JP, Blow JJ, Inagaki N, Inagaki M, Delcros JG, Moulinoux JP (1997) Biochemical and cellular effects of roscovitine, a potent and selective inhibitor of the cyclin-dependent kinases cdc2, cdk2 and cdk5. *Eur J Biochem* 243:527–536. [CrossRef Medline](#)
- Müller M, Pym EC, Tong A, Davis GW (2011) Rab3-GAP controls the progression of synaptic homeostasis at a late stage of vesicle release. *Neuron* 69:749–762. [CrossRef Medline](#)
- Odajima J, Wills ZP, Ndassa YM, Terunuma M, Kretschmannova K, Deeb TZ, Geng Y, Gawrzak S, Quadros IM, Newman J, Das M, Jecrois ME, Yu Q, Li N, Bienvenu F, Moss SJ, Greenberg ME, Marto JA, Sicinski P (2011) Cyclin E constrains Cdk5 activity to regulate synaptic plasticity and memory formation. *Dev Cell* 21:655–668. [CrossRef Medline](#)
- Ryan TA (1999) Inhibitors of myosin light chain kinase block synaptic vesicle

←

(Figure legend continued.) treatment with CSA (top) or unsilenced after treatment of Ros (bottom). Scale bar, 5 μ m. **B**, Corresponding traces of silenced (white circle in **A**, top) and unsilenced (white circle in **A**, bottom) boutons with or without treatment of CSA or Ros. **C**, Histogram of the fraction of silent and responsive boutons measured by GCaMP3 in WT with or without CSA or roscovitine: WT_{silent} = 0.17 \pm 0.04, WT_{responsive} = 0.83 \pm 0.04 (n = 25), WT + CSA_{silent} = 0.46 \pm 0.09, WT + CSA_{responsive} = 0.54 \pm 0.09 (n = 9), WT + Ros_{silent} = 0.07 \pm 0.02, and WT + Ros_{responsive} = 0.93 \pm 0.02 (n = 16). **D**, Histogram of the proportion of silent and responsive boutons measured by MgGreen in WT with or without CSA or Ros. The division of silent or responsive boutons was based on a signal-to-noise ratio of 1 (peak vs SD of baseline) for the 1AP response: WT_{silent} = 0.14 \pm 0.03, WT_{responsive} = 0.86 \pm 0.03 (n = 19), WT + CSA_{silent} = 0.36 \pm 0.11, WT + CSA_{responsive} = 0.64 \pm 0.11 (n = 7), WT + Ros_{silent} = 0.04 \pm 0.02, and WT + Ros_{responsive} = 0.96 \pm 0.02 (n = 10). **E**, Histogram of the fraction of silent boutons measured by GCaMP3 and normalized to fraction of WT silent boutons in WT, CNA α KD, CDK5KD, WT with/without CSA or roscovitine, and WT with ω -conotoxin GVIA (Cono) or ω -agatoxin IVA (Aga) with/without roscovitine: WT = 1.0 \pm 0.18 (n = 25), CNA α KD = 3.00 \pm 0.24 (n = 26), CDK5KD = 0.36 \pm 0.09 (n = 12), WT + CSA = 2.70 \pm 0.54 (n = 9), WT + Ros = 0.40 \pm 0.09 (n = 16), WT + Cono = 3.31 \pm 0.66, WT + Cono + Ros = 2.85 \pm 0.60 (n = 7), WT + Aga = 1.87 \pm 0.16, and WT + Aga + Ros = 0.76 \pm 0.40 (n = 8).

- pool mobilization during action potential firing. *J Neurosci* 19:1317–1323. [Medline](#)
- Su SC, Seo J, Pan JQ, Samuels BA, Rudenko A, Ericsson M, Neve RL, Yue DT, Tsai LH (2012) Regulation of N-type voltage-gated calcium channels and presynaptic function by cyclin-dependent kinase 5. *Neuron* 75:675–687. [CrossRef Medline](#)
- Sun T, Wu XS, Xu J, McNeil BD, Pang ZP, Yang W, Bai L, Qadri S, Molkentin JD, Yue DT, Wu LG (2010) The role of calcium/calmodulin-activated calcineurin in rapid and slow endocytosis at central synapses. *J Neurosci* 30:11838–11847. [CrossRef Medline](#)
- Takahashi T, Momiyama A (1993) Different types of calcium channels mediate central synaptic transmission. *Nature* 366:156–158. [CrossRef Medline](#)
- Tedford HW, Zamponi GW (2006) Direct G protein modulation of Cav2 calcium channels. *Pharmacol Rev* 58:837–862. [CrossRef Medline](#)
- Tian L, Hires SA, Mao T, Huber D, Chiappe ME, Chalasani SH, Petreanu L, Akerboom J, McKinney SA, Schreier ER, Bargmann CI, Jayaraman V, Svoboda K, Looger LL (2009) Imaging neural activity in worms, flies and mice with improved GCaMP calcium indicators. *Nat Methods* 6:875–881. [CrossRef Medline](#)
- Yan Z, Chi P, Bibb JA, Ryan TA, Greengard P (2002) Roscovitine: a novel regulator of P/Q-type calcium channels and transmitter release in central neurons. *J Physiol* 540:761–770. [CrossRef Medline](#)
- Zeng H, Chattarji S, Barbarosie M, Rondi-Reig L, Philpot BD, Miyakawa T, Bear MF, Tonegawa S (2001) Forebrain-specific calcineurin knockout selectively impairs bidirectional synaptic plasticity and working/episodic-like memory. *Cell* 107:617–629. [CrossRef Medline](#)
- Zhao C, Dreosti E, Lagnado L (2011) Homeostatic synaptic plasticity through changes in presynaptic calcium influx. *J Neurosci* 31:7492–7496. [CrossRef Medline](#)